Emiliania huxleyi virus arrests host calcification and nutrient consumption, and triggers shifts in organic stoichiometry

Tamar Dikstein[a,b], Gilad Antler[c,b,], Andre Pellerin[d], Shlomit Sharoni[e], Miguel J. Frada[a,b,1]

[a]Department of Ecology, Evolution and Behavior, Silberman Institute of Life Sciences, The Hebrew University of Jerusalem, Jerusalem, Israel

[b]The Interuniversity Institute for Marine Sciences in Eilat, Eilat, Israel

[c]Department of Earth & Environmental Sciences, Ben-Gurion University of the Negev, Beersheba, Israel

[d]Institut des sciences de la mer, Université du Québec à Rimouski and GEOTOP, Rimouski, Québec, Canada

[e]Department of Earth, Atmospheric and Planetary Sciences, Massachusetts Institute of Technology, Cambridge, United States of America

Corresponding author: miguel.frada@mail.huji.ac.il

Keywords: Coccolithophore, Virus, Nutrient uptake, Calcification, Elemental stoichiometry.

Abstract

Blooms of the dominant coccolithophore *Emiliania huxleyi* are routinely infected by a specific lytic virus (EhV), which rapidly kills host cells triggering bloom termination and organic and inorganic carbon export. However, the impact of EhV on the dynamic of resource acquisition and cellular stoichiometry remains unknown, limiting the current understanding of the ecological and biogeochemical significance of *E. huxleyi* blooms. To tackle this knowledge gap, we used algal and EhV cultures to determine over the course of infections the dynamics of alkalinity, modulated by calcification, nitrate and phosphate consumption and organic matter stoichiometry. We found that within 24hr alkalinity concentration stabilized and nutrient uptake declined to background levels. In parallel, the stoichiometric ratio of carbon to nitrogen increased and the nitrogen to phosphorus ratio declined. These variations likely resulted from lipid accumulation

required for viral replication and the differential retention of phosphorus-rich macromolecular pools in decaying cells, respectively. Finally, during post-infection and decline of the host population, a progressive enrichment in phosphorus relative to nitrogen and carbon was measured, detected in the remaining cell lysates. We estimate that this stoichiometric shift is driven by the accumulation of heterotrophic bacteria involved in the degradation of organic material. Viral-mediated cell remodeling and consequent shifts in biomass stoichiometry likely impacts the patterns of nutrient cycling and biological carbon pump efficiency during large-scale blooms in the oceans.

Introduction

Phytoplankton are a taxonomically diverse group of photosynthetic microorganisms that inhabit the sunlit layer of the oceans where they are responsible for about 45% of global primary production and for driving the biological carbon pump (1). This latter process results in a net drawdown of atmospheric CO_2 into the ocean's interior, henceforth influencing global climate (2). Biogeochemical cycles of the major nutrients (nitrogen; N and phosphorus; P) and carbon (C) are interlinked (3, 4). The ratio of N to P in seawater determines which nutrient limits biological productivity in the ocean, with cascading effects on the marine food web (5–7). In addition, the ratio of carbon to the limiting nutrient in organic matter, determines the maximum amount of carbon that can be fixed and exported (8). By consequence, phytoplankton elemental stoichiometry is a main component regulating the efficiency of the biological carbon pump.

Viruses are ubiquitous regulators of microbial growth and evolution in the oceans (9, 10). Mortality caused by lytic viruses is estimated to influence marine primary production, food-web dynamics and nutrient cycles in the oceans (11, 12). However, to our knowledge little is known on the impact of viral infections on phytoplankton and particulate organic carbon stoichiometry. Quantifying the impact of viral infection on nutrient cycling in phytoplankton cells is critical to improve our understanding of marine ecosystem functioning, biogeochemical cycles and the potential feedback on the global climate. Here, we address the impact of viral infections in *Emiliania huxleyi*, a cosmopolitan unicellular calcifying photoautotrophic organism belonging to the coccolithophore clade and capable of forming large-scale blooms in the oceans. Coccolithophores are an important group of marine phytoplankton estimated to contribute 1% to 10% of primary production and phytoplankton biomass, increasing up to

40% during bloom conditions (13, 14). As a characteristic, coccolithophores produce an outer covering of calcite plates termed coccoliths (15, 16). This attribute confers coccolithophores a unique functional role in pelagic ecosystems. The biosynthesis of coccoliths is an energy costly process involving the active transport of the calcification substrates, Ca^{2+} and HCO^{-}_{3}, dissolved in seawater into the cell where coccoliths are precipitated (16). In doing so, coccolithophores reduce both seawater total dissolved inorganic carbon (DIC) and alkalinity, which changes the equilibrium between the different DIC forms and reduces the potential for seawater CO_2 uptake and to buffer for pH changes (17). Moreover, the biological precipitation and export of calcite results in a net release of CO_2 to the atmosphere, a mechanism referred to as the alkalinity pump (or carbonate counter pump), which counter acts the biological carbon pump. Nonetheless, the impact of any CO_2 production during calcification may be offset through the ballasting of organic carbon by heavy coccoliths entangled in marine snow, which can increase the efficiency of the biological carbon pump (17, 18). The relative strength of the two pumps, represented by the so-called rain ratio, determines to a large extent the air/sea exchange fluxes of CO_2 and the magnitude of oceanic carbon sequestration, with important effects on the biogeochemical cycling of carbon and climate (17, 19).
In this context, blooms of *E. huxleyi* bear a significant impact. These blooms are typically extensive and develop over several weeks in temperate and subpolar waters during late spring/early summer periods (20–22). The underlying conditions for bloom formation are numerous and may vary between sites, thus a matter of debate (21, 23). However, bloom decline is linked to an important extent to lytic infections by a specific *E. huxleyi* virus (EhV) (24–27), a large double-stranded DNA Coccolithovirus (28). At the cellular level, EhV infection leads to profound remodelling of the *E. huxleyi* metabolism to support viral proliferation. These include the activation and recruitment of the host's oxidative stress (29–31), upregulation of autophagy, nuclear degradation (32), and both enhance glycolytic fluxes and lipid biosynthesis (33). The latter include triacylglycerols (33, 34) and specific virus-derived glycosphingolipids that are important structural components of EhV particles and chemical signals triggering host's programmed cell death (30, 33). Additionally, EhV infection prompts coccolith shedding from the cell surface, changing the optical signature of infected populations (35–37), and stimulates the production of transparent exopolymer particles (TEP) that can form large aggregates

entrapping cells and coccoliths and enhance the vertical export flux of both particulate organic and inorganic carbon (38, 39).

Although focus has been directed to viral-mediate changes in metabolic and structural properties of host *E. huxleyi* cells, the impact of EhV on nutrient uptake, calcification dynamics and ultimately on the basal elemental stoichiometric compositions (C:N:P) of the viral infected cells (i.e., virocells, (40)) remains to be tested. This limits our understanding of basic feature of the host-virus interplay between *E. huxleyi* and EhV and bloom turnover, and the impact of viral infection on carbon export. To tackle this knowledge-gap, we examined the dynamic of macronutrient (N and P) consumption and calcification during viral infections, as well as the C:N:P stoichiometric composition of infected populations in controlled culture conditions. Our study demonstrates the impact of virus on the regulation of nutrient incorporation and cellular composition of *E. huxleyi* virocells and provide key insights on ensuing ecological and biochemical consequences of large-scale viral infections during oceanic blooms.

Results

Algal growth and variations in optical properties

Detailed survey of viral infections was monitored during 72 hr (Fig. 1). The cell growth developed comparably in infections and controls during the first 36 hr reaching a density of around 1.25 x 10^6 cells mL^{-1}. The growth rate over first day averaged ~0.5 ± 0.06 day^{-1} in both treatments. During the second day, concurrent exponential accumulation of virions was detected in the infected cultures. Peak viral densities were detected 48 hr post-infection (~ 2.7 x 10^8 virions mL^{-1}). The estimated viral burst size was estimated to be ~230 viral particles $cell^{-1}$. In parallel, cell density declined down to 0.5 x 10^6 cells mL^{-1} by 72 hr, while the control cultures reached the stationary growth phase (~ 2.0 x 10^6 cells mL^{-1}) (Fig. 1A).

Average chlorophyll autofluorescence and side scatter measured by flow cytometry were used to as indicators of cell health and degree of cell calcification. During exponential growth, both parameters commonly oscillate through day-night cycles due to cell enlargement and coccolith buildup during exponential growth (41). This was detected during the first day in both treatments. However, during the second day these diel oscillation in optical signals stopped and overall declined (Fig. 1B–C). A slight increase in the average side scatter signal was detected at 72hr, can be explained by the

formation of aggregates of decaying cellular materials with high scattering properties, not from the growth of living cells.

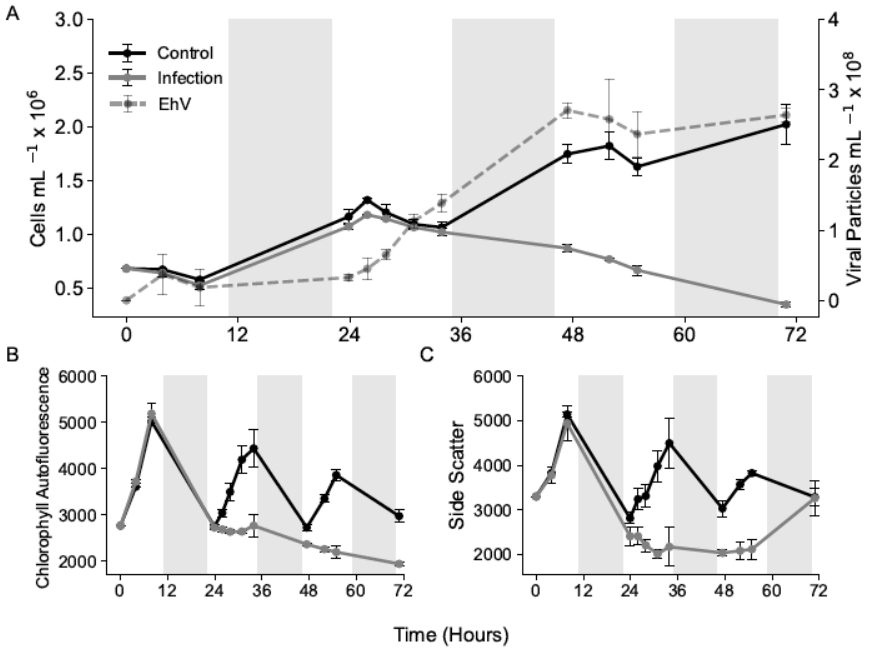

Figure 1. Algal and viral growth and variations in chlorophyll autofluorescence and side scatter. *E. huxleyi* cultures were infected with EhV 201 and compared with noninfected control cells. (A) Cell growth and extracellular viral production. (B) Mean population values of Red autofluorescence. (C) Mean population values of side scatter. The x-axes correspond to hours post infection. Grey sections represent the night period and dots indicate mean values of each treatment (Control/Infection), Error bars represent standard error of replicates, n=3.

Alkalinity, nitrate and phosphate consumption

During the first day, the consumption of alkalinity (Fig. 2A), nitrate (Fig. 2B) and phosphate (Fig. 2C) was broadly similar in infected and control cultures. During the first light phase alkalinity, nitrate and phosphate consumption averaged 13.40 ± 0.90 µmol L^{-1} h^{-1}, 3.1 ± 0.4 µmol L^{-1} h^{-1} and 0.12 ± 0.06 µmol L^{-1} h^{-1}, respectively. During the first dark period the consumption of alkalinity was much lower (avg. 1.6 ± 0.8 µmol L^{-1} h^{-1}), nitrate was about half (avg. 1.20 ± 0.20 µmol L^{-1} h^{-1}), and phosphate identical to light period (avg. 0.11 ± 0.01 µmol L^{-1}). Overall, this was a period where cell growth was identical in infected and control cultures. However, between 24hr and 36hr post-infection coincident with the arrest of cellular optical signals, alkalinity was halted and nutrient

consumption declined to very low background levels (Fig. 2A). After 36hr nitrate and phosphate uptake were both arrested.

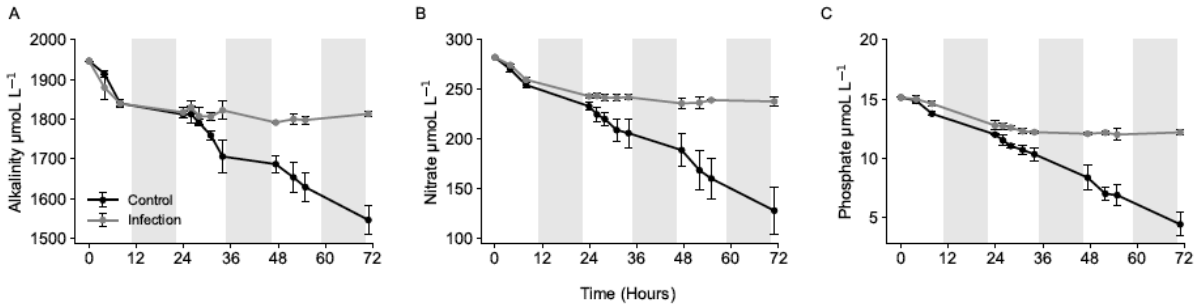

Figure 2. Dynamic of Alkalinity, nitrate, and phosphate in control and infected *E. huxleyi* cultures. The measured concentration of control and EhV infected cultures; (A) Alkalinity. (B) Dissolved nitrate. (C) Dissolved phosphate. The x-axes correspond to hours post-infection. Grey sections represent the night period and dots indicate the mean values of each treatment (Control/Infection), Error bars represent the standard error of replicates, n=3.

Particulate organic matter and stoichiometry dynamics

To determine the effect of viral infection on the elemental composition of coccolithophore cells, POC, PON, and POP were quantified over the length of the infection (72hr). An additional experiment was set to determine the longer-term variations in the elemental composition of cell-derived lysates over 13 days post-infection (333 hr). Both experiments were set up at the exact conditions and the output was nearly identical, thus presented together (unless otherwise indicated). POC, PON, and POP per cell as determined at the start of the experiment were 5.45 ± 0.15 pg cell^{-1}, 1.22 ± 0.06 pg cell^{-1} and 0.14 ± 0.003 pg cell^{-1}, respectively. However, EhV infections result in very heterogeneous cultures, including cells in different physiological states, dead cells (33), TEP (38), and aggregates (42), all of which bear a particulate organic matter (POM) signature. Thus, the particulate organic C, N, and P (POC, PON, and POP, respectively) are presented per unit volume to illustrate the temporal variations in the ensemble of particulate components produced during viral infected and control cultures and not per cell basis (Fig.3). The stoichiometric ratios are presented in Fig. 4, focusing separately on the infection period and post-infection for better visual details of variations during infections.

Over the infection period, the variations in cell and viral densities (Fig. 3A) were broadly identical to what was shown before in Fig. 1A. Briefly, the infected cultures increased in density equally to controls over the first 24hr and then decline to background densities $<10^3$ cell mL^{-1}. Free EhV rapidly peaked by the end of the second day (~3.50 x 10^8 virions mL^{-1}). Viral densities remained relatively stable until day 13. The control populations multiplied exponentially over the first 120hr and then transitioned to stationary growth phase at a density of about 4 x 10^6 cell mL^{-1}. In parallel, cohabiting bacteria progressively accumulated in the cultures (Fig. 3B). The increase in the bacterial population was higher in infected cultures doubling by t = 96hr (~0.40 x 10^8 bacteria mL^{-1}) the density from the controls. The bacterial density kept increasing, reaching in infected cultures twice as higher densities (~0.9 x 10^8 bacteria mL^{-1}) than in the controls by day 13.

In control cultures, POC, PON, and POP concentrations progressively increased during the exponential phase as biomass accumulated (Fig. 3C–-E). Then PON and POP stabilized as cultures entered stationary growth. In parallel, the molar stoichiometric ratios remained relatively stable during exponential growth and then C:N and C:P both increase during exponential growth (Fig. 4). By contrast, in the presence of EhV the POC, PON, and POP concentrations increased during the first day of infection, but then rapidly declined concomitant with cell demise. During this first infection period, variations in the elemental stoichiometry relative to the controls were identified. Namely, the C:N ratio was significantly higher (C:N > 8.0) in infected cultures at 48hr and 72 hr post-infection than in the controls (C:N ~ 6.7) (Fig. 4A). By contrast, over the same period the average N:P was lower in infected cultures (N:P 14.0–15.5) than in the control ones (N:P 15.7–16.2) (Fig. 4E). In the post-infection period, a slight increase of POC, PON, and POP density was detected until the end (Fig. 4B, D and F). However, in parallel, negative trends were detected for the C:N ratio (R^2 = 0.91) and C:P ratio (R^2 = 0.37), indicating a progressive enrichment of N and P relative to carbon in organic biomass post-infection.

Bacterial stoichiometry often deviates from the typical phytoplankton Redfield Ratio. Average bacterial C:P is 77 and C:N is 4.9, while N:P is 17, similar to phytoplankton (43, 44). Thus, to test whether the observed shift in POM stoichiometry post-infection could result from the recycling of algal to bacterial biomass and accumulation of high bacterial titers, we calculated the contribution of bacteria over the course of our experiment. The

results indicate that by the end of the infection on day 3 (72 hr), bacteria biomass contributed already around 30%, at day 7 (168 hr) nearly 60%, and by day 13 nearly 80% of the total measured POM (Fig. 5).

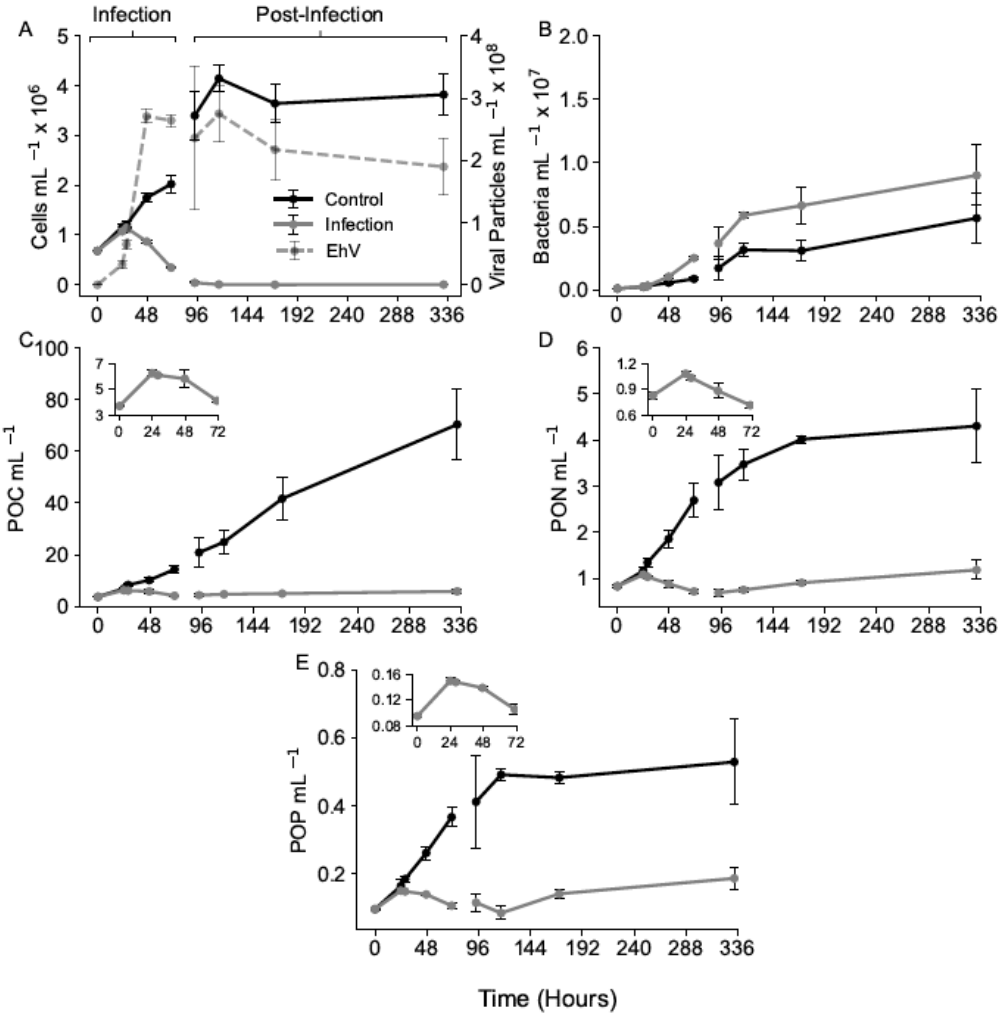

Figure 3. Variations in particulate organic matter (POC, PON, POP) in control and EhV-infected *E. huxleyi* cultures. Between 0 hr and 72 hr concerns the infection period. After 96 hr concerns the post-infection period (see the main text for details). (A) Cell and viral densities. (B) Free bacterial densities (C–E) POC, PON, and POP concentrations, respectively. For higher detail, inset figures overlapping C, D and E highlight the variations in POC, PON, and POP during the infection period. Error bars represent the standard error of replicates, n=3.

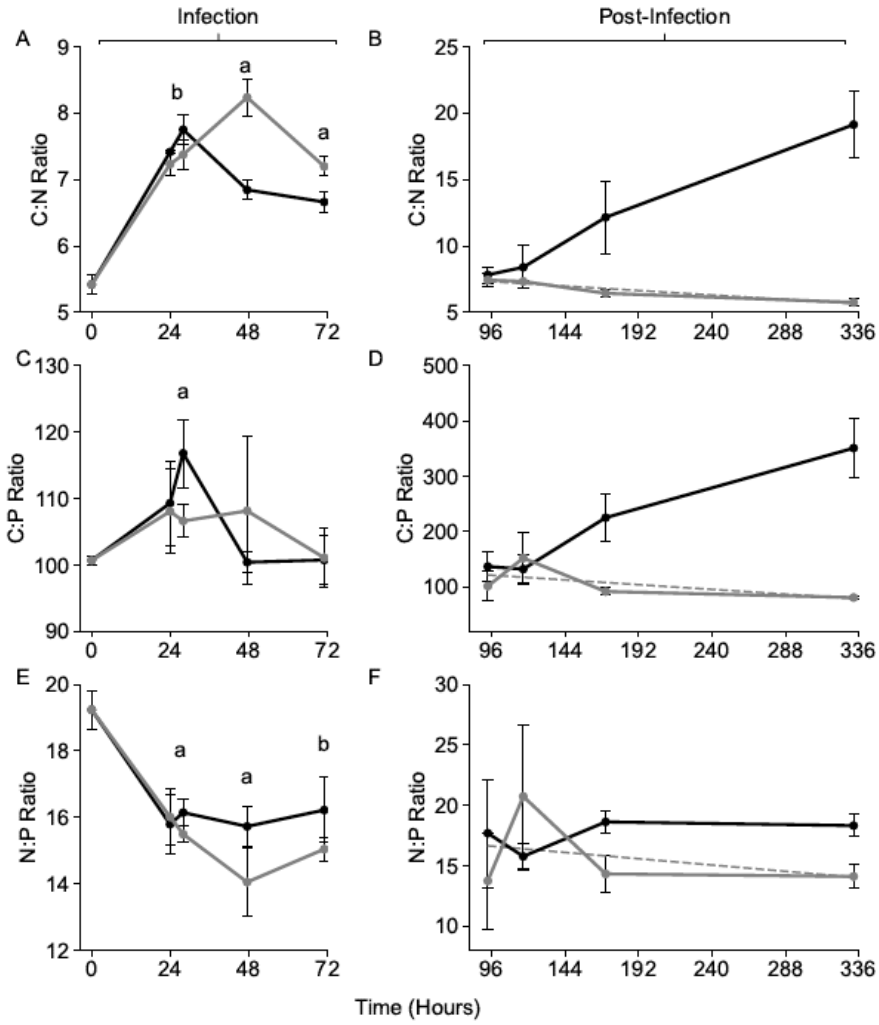

Figure 4. Variations in the elemental stoichiometric ratios (C:N, C:P, and N:P) in control and EhV-infected *E. huxleyi* cultures. The infection period (0-72 hr; A, C, and E) and post-infection period (from 96 hr to 333 hr; B, D, and F) are presented separately for better visualization. Respectively, the equations and R^2 values of the linear regressions during the post-infection period for C:N, C:P and N:P are: $y = -0.16x + 7.98$, $R^2 = 0.91$; $y = -4.28x + 138.39$, $R^2 = 0.37$; $y = -0.26x + 17.65$, $R^2 = 0.12$. Error bars represent the standard error of replicates, n=3. Statistical significance is indicated by the superscript letter a ($p < 0.05$) and b ($p < 0.1$).

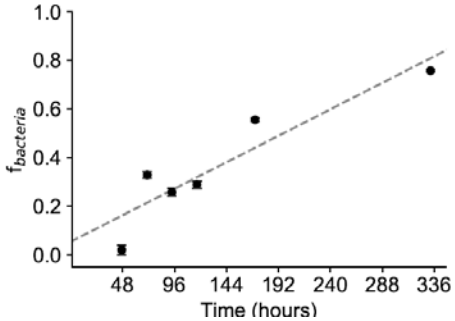

Figure 5. Mathematical estimates of the contribution of bacteria to particulate organic matter over the course of the infection and post-infection periods as defined in Fig. 3 and 4. The quadratic fitting describes the rate of bacterial accumulation, which is a saturation function (f_{bacteria} cannot exceed 1; y = 0.054x + 0.054, R^2=0.85).

Discussion

EhV halts calcification and nutrient uptake in infected host cells

A typical dynamic of *E. huxleyi* (RCC 1216) by the specific EhV 201 set at an MOI of 0.2 was detected (45, 46). Broadly, during the second day of infection, the daily oscillations of Chl fluorescence and side scattering signals were both halted and gradually declined in intensity (Fig. 1). These responses are consistent with the decline in the cellular chlorophyll content, impaired photophysiology (47–50), and coccolith shedding triggered during EhV infections (37). Then, after 36hr, the cell growth abruptly declined as a consequence of EhV-mediated cell death (29, 30). A primary goal of this study, was to test the impact of EhV infection on 1) calcification as detected by determining the draw-down of alkalinity levels in the medium and 2) on the intake of the major macronutrients (nitrate and phosphate). During the first day, calcification was comparable between infected and control cultures. Alkalinity draw-down occurred during the light period, but not through the night period (Fig. 2A). However, on the second day of infection, calcification was completely arrested. This coincided with the onset of viral burst and the overall shift in Chl fluorescence and side scatter signals in infected populations (Fig. 1). Coccolith biosynthesis is a complex energy-demanding mechanism requiring abundant lipid membranes for the coccolith vesicles and the secretion system that ultimately results in large inorganic structures seemingly unnecessary to viral replication (16). Thus, it is plausible that the viral-mediated breakdown of photosynthesis and the rapid progression of EhV, requiring large fluxes of nucleotides, lipidic resources, and energy,

naturally results in the cessation of calcification and the incapability of coccolithophore virocells to keep and restore the disintegrating coccosphere.

As for calcification, nitrate and phosphate were both consumed during the first day in both control and infected cultures (Fig. 2B–C). However, in contrast to calcification, nutrient consumption continued through the dark period. Dark uptake of nitrate is known for *E. huxleyi* (41). Reports on the dark uptake of phosphate are less clear (41, 51). However, a higher affinity for phosphate has been described during the night, likely due to higher requirements for cell division (52). Nutrients acquired up to this stage through the infection are naturally incorporated into EhV biosynthesis as has been recently demonstrated in isotopic labeling experiments with carbon and N (53, 54). The reliance of EhV on external phosphate has not been thus far assessed, but likely follows analogous trends facilitated by the activity of a viral phosphate permease gene encoded by some EhV strains (55, 56). During the second day nutrient consumption was arrested. This occurred as side scatter and chlorophyll signals stopped oscillating, but prior to viral burst and cell decline. This suggests that at this stage the virocell reached the final stages of viral maturation, and that any further metabolic and energetic requirements mostly relied on intracellular recycling of available macromolecules.

EhV-mediated shifts in biomass stoichiometry during infection and post-infection

In control cultures, as expected, POC, PON, and POP per unit volume increased over time as biomass accumulated until the cultures reached the stationary phase and PON and POP stabilized. During the exponential growth phase, the C:N, C:P and N:P stoichiometry were fairly constant and close to the Redfield ratio through the exponential growth phase, but once the cultures entered the stationary phase the C:N and C:P rapidly increased (Fig. 4). This is likely caused by the accumulation of C-rich lipids in nitrate and phosphate limited cells (57). By contrast, the concentration of POC, PON, and POP declined during the infection period, which can be essentially attributed to the viral-mediated cell lysis and loss of cellular contents to the medium as dissolved organic matter. Over this first infection period, a consistent increase in C:N and a decline in N:P ratios were detected over multiple time points, indicating both an enrichment of C and P during infection (Fig. 4). The first stoichiometric shift likely results from the well-documented intracellular accumulation of C-rich lipids in infected *E. huxleyi* cells (33, 34, 58). The second stoichiometric shift is less clear. A comparable shift in elemental

composition during viral lysis has been detected in the “brown tide” chrysophyte *Aureococcus anaphagefferens* (59). In that system, carbon showed the largest proportional release to the dissolved phase following viral lysis. It was argued that this likely derived from the relative predominance of carbon in algal cytoplasm that could easily leak out to the medium following cell decay and bacteria consumption. An important loss of dissolved carbon in *E. huxleyi* during infection has also been also recently estimated (60). By contrast, in *A. anaphagefferens*, N and P were both more retained in the particulate fraction. Nitrogen was possibly rapidly transferred to the bacterial community, which we cannot argue for *E. huxleyi* during infection here the relative importance of N to the elemental stoichiometry declined, while P was suggested to be retained in large structural components of the algae (59), as for example lipid membranes. This may be the case in *E. huxleyi* as well, which have been shown to bear a more important fraction of phospholipids than control cells (34). The contribution from mRNA that likely builds up during viral propagation may also be important to P enrichment during infection. In contrast, viral biomass likely did not influence the overall organic matter proportions and ratios. For instance, using the similar *Paramecium bursaria Chlorella virus*-1 (PBCV-1) with estimated C:N:P stoichiometry of 17:5:1 and mass of 1×10^9 Da (61, 62), we estimate that during the second day, the contribution of Ehv accumulated inside the infected cells prior to burst (~230 virions per cell) would represent a nearly undetectable fraction ($< 1 \times 10^{-8}$ %) to the total particulate organic C, N or P harvested. In any case, a future detailed examination of the elemental redistribution between cell, viral, and bacterial compartments and the composition and dynamic of macromolecules should enable us to decipher the underlying process of stoichiometric shifts detected here. However, the fact that overall stoichiometric changes occurred during day 2 and 3 (48 hr-72 hr), which was after nutrient consumption stopped, further suggest the prevalence of the internal recycling of cellular and macromolecular pools to fuel viral proliferation relative to *de novo* intake of resources. Post-infection, when remaining coccolithophore cell abundance was very low (10^3–10^4 cell mL^{-1}) and the cultures were visibly full of large aggregates (see (42)), POM concentrations progressively bounced back to nearly initial values. In parallel, the C:N and C:P significantly declined, indicating an enrichment in N and P relative to C in the remaining organic matter. We use a stoichiometric approach to estimate bacterial accumulation, as we counted free bacteria and not POM-associated bacteria. Our

estimates (Fig. 5) indicate that these trends likely resulted from the rampant accumulation of heterotrophic bacteria that have considerably higher demands in N and P relative to C (C:N= 4.9; C:P=77.0) than phytoplankton (43, 44). Thus, heterotrophic bacteria, triggered by viral-mediated lysis, accumulate at high rates in remaining cell-aggregated. Such an accumulation, leads to a significant replacement of algal biomass by bacterial biomass in the decaying particulate organic matter.

Potential ecological and biogeochemical implications of EhV infections

During *E. huxleyi* infections, large fractions of organic matter are lost to the dissolved phase as detected by marked POC, PON, and POP concentration decline (Fig. 3). The rapid release of cell contents during infections, as part of the so-called 'viral shunt' (9, 10), triggers the rapid rise of bacterial communities that can actively benefit from the break-down and reuse of dissolved elements and lysates as it has been shown in other host-viral systems (e.g., (59)). In parallel, stoichiometric variations were detected relative to non-infected cells (Fig. 4). In the short term, during the course of infection and population decline, an enrichment in C and P relative to N was detected, which can be directly attributed to the EhV replication cycle and underlying metabolic remodeling of virocells. In the longer term, decaying organic matter of *E. huxleyi* cells appears to be progressively replaced to a large extent by bacterial biomass likely bound to aggregates (42) produced during the earlier infection. The current view is that the formation of coccolith-dense aggregates during *E. huxleyi* blooms infected by EhV can enhance the carbon export efficiency, following the 'viral shuttle' model (39, 63, 64). However, modifications in the elemental composition can impact the efficiency of carbon export. Rapid export of recently infected populations with high carbon ratios may indeed benefit the efficiency of carbon export. By contrast, slow export or resuspension of lysates in more turbulent settings could enable time for the accumulation of bacteria and concomitant enrichment of P relative to carbon in exported material, which then could in fact attenuate the magnitude of the biological carbon pump by lowering the relative contribution of carbon to exported biomass (6, 8, 65).

Taken together, it seems that the counteracting effect of viral shunt and viral shuttle likely operate simultaneously during the interplay between *E. huxleyi* and EhV, as it is most likely the case for most viral-host systems in the oceans. Yet, their relative importance and efficiencies as well as comprehensive exploration in natural blooms

stoichiometry and export dynamics are required to validate our culture-based results and determine the significance of *E. huxleyi* blooms in export production in the oceans. To this, one must join the impact of grazing on this complex dynamic. In fact, *E. huxleyi* blooms are targeted by microbial and zooplankton consumers (39, 57, 66–68) as well as eukaryotic osmotrophs (60), all of which can contribute to the consumption of infected cells and lysates and can further influence carbon export efficiencies. On this topic, differences in regard to susceptibility to grazing between infected and non-infected cells in *E. huxleyi* have been observed (69–71). In a recent study, lower ingestion rates by the heterotrophic dinoflagellate *Oxyrrhis marina* in EhV-infected cells were determined. However, despite lower ingestion, *O. marina* displayed higher growth rates, which suggests higher nutritional values and/or great assimilation of infected cells (71). The stoichiometric shift observed in our study indicates however that such nutritional value can rapidly change depending on the state of the infection, which in turn could affect the efficiency of the marine food web feeding during blooms.

Finally, as detailed above, calcification rapidly stalled during infection. Consequently, the consumption of dissolved carbonate ions also should stop as it stops the draw-down of seawater alkalinity as we observed experimentally. This highlights the antagonistic role of EhV infection on the marine carbon counter pump, reducing the net increase of dissolved CO_2 by demising growing populations with high rates of calcification and consequently upholding the buffer capacity of the oceans (17).

Concluding remarks

In this study, we demonstrate that EhV infection arrests *E. huxleyi* calcification, nutrient acquisition and caused ensuing shifts in the stoichiometry of organic matter. These included both a short-term shift during active viral infection and a long-term shift driven by cohabiting bacterial communities actively consuming cell-derived lysates and aggregates. During natural blooms, the dynamic of EhV infections can be rapid, but also heterogeneous between different blooming areas (39). Thus, one can expect the stoichiometric seascape to be very variable. Nonetheless, such viral-mediated changes in the nature of exported materials, likely influence the cycling of elemental in the photic layer and the export efficiency of biomass to the deep ocean during large-scale coccolithophore blooms. Further studies are required to validate our observation in natural coccolithophore populations. However, our study demonstrates that assessing

the impact of viral infections on the elemental biogeochemistry of phytoplankton biomass is crucial to determine their role and impact on the marine ecosystem.

Materials and Methods

Cell culturing and viral-infections

The xenic calcifying *E. huxleyi* strain RCC1216 (diploid) was used in all experiments. Cell cultures were set in seawater-based K/2 (minus ammonium) medium (72), at 18°C, 13h:11h light: dark cycle, respectively, 80 µmol quanta m^{-2} s^{-1} irradiance using a warm white LED system and gently air-bubbled through 0.2 µm filter. A 6 L stock culture was grown for 3 days and then subdivided into six replicate glass bottles of 1 L each. Three of the replicates were infected with EhV 201 at a Multiplicity of infection (MOI) of 0.2, and three other replicates were used as non-infected controls. Sub-samples for cell, bacterial and viral counts, nitrate, phosphate, and alkalinity, as well as POC, PON, and POP, were collected at different time points with high frequency in the first 72hr post-infection. An additional experiment run over 13 days was used to determine long term changes in POC, PON, and POP. See the details for sampling and analyses below.

Cell, virus, and bacterial counts

E. huxleyi, bacteria, and EhV particles were enumerated by flow cytometry (Attune NxT, Life Technology). Algal cells were identified based on chlorophyll fluorescence (excitation 488 nm) and side scatter (46, 73). The mean side scatter and chlorophyll autofluorescence values were used as indicators for the degree of cell calcification (coccolith covering) and cell health, respectively. For viral and bacterial counts, samples of 0.5 mL were fixed with 0.5% glutaraldehyde and counterstained with 1:10000 SYBR Green (Invitrogen). Viruses and bacteria were identified by flow cytometry based on the green fluorescence (excitation: 488 nm and emission: 530–737 nm) and side scatter (73). The cell growth rate was determined as the natural logarithm of the cell density at 0 and 24hr divided by time. Viral burst size, was determined as the number of viruses released per lysed cell (estimated as the ratio of the maximal number of viruses produced to the maximum cell concentration reached by the specific host before cell decrease) (24, 35).

Inorganic Nutrients and alkalinity

Duplicate samples of 10 mL were filtered through 0.2 µm filters (Sterivex, Millipore) and kept at 4˚C until further analysis. Alkalinity was measured by acid-base titration following (74), via automatic titrator (Titroline 7000 Si analytics), and calculated using a gran plot with a precision lower than 20 mEq. Phosphate (as dissolved reactive phosphate) was measured by colorimetric spectroscopy using the Mo-Blue method (Cary 8454 UV-vis spectrometer, Agilent) with a precision of 0.1 mM and detection limit of 0.1 µM (75). Nitrate was measured by second-derivative spectroscopy (Cary 8454 UV-vis spectrometer, Agilent) with a precision of 0.1 mM and detection limit of 0.1 µM (76).

Particulate organic carbon, nitrogen, and phosphorus

For POC and PON, 20 mL duplicate samples were collected and filtered under low-pressure vacuum filtration (100 mm Hg) onto pre-combusted (450˚C, 5hr) Whatman GF/F filters (25 mm diameter, 0.7 µm effective pore size). Then the filters were rinsed with 230 µL of 1M hydrochloric acid (HCl) to remove particulate inorganic carbon (PIC), oven-dried overnight at 65˚C, and folded into tin capsules. Carbon and nitrogen content analyses were conducted in Continuous-flow Isotope Ratio Mass Spectrometry (CF-IRMS) using a Deltaplus XP mass spectrometer (ThermoScientific) coupled to an elemental analysis (EA) COSTECH 4010 (Costech Analytical) equipped with a zero blank autosampler. For every 36 samples or less, 10 secondary standards are used to correct the data using a linear correction. Caffeine, nannochlopsis, and Mueller Hinton broth were used as secondary standards calibrated from NIST primary standard. Analytical error (n=50) on measurement was 0.06‰ and 0.08‰ for 6N and 6C, respectively. System suitability prior to analysis was evaluated using the standard deviation of zero reference gas (N and carbon dioxide) over 10 measurements and the maximum acceptable variation was set to 0.06%. Certified reference material from Elemental Microanalysis treated as a sample is used as quality control. Quantification is based on external secondary standards with a calibration range of 0.025 mg to 0.250 mg and 0.040 mg to 0.400 mg for nitrogen and carbon respectively according to (Agnihotri et al., 2014). For POP, 50 mL duplicate samples were filtered under low-pressure vacuum filtration (100 mm Hg) onto pre-combusted (450˚C, 5hr) Whatman GF/F filters (25 mm diameter, 0.7 µm effective pore size). They were then combusted at 450˚C, for 5hr in a muffle furnace, cooled down, and immersed in 10 ml of 0.5N of HCl for 60 min at 90˚C in

a heating block (77). Finally, 5 ml of supernatant was volumetrically subsampled into 15 ml centrifuge tubes for colorimetric spectroscopy using the Mo-Blue method (Cary 8454 UV-vis spectrometer, Agilent) as mentioned earlier for the analysis of inorganic P.

Mathematical estimation of bacterial contribution to particulate organic matter

Given the rampant accumulation of free bacteria during the infection experiments (see Fig. 3), it is most likely that there was a concomitant accumulation of bacteria attached to particulate organic matter (60). POM-bound bacteria were not measured. Thus, we estimated the contribution of bacteria to total particulate organic matter over the course of the experiment using a stoichiometric approach. These calculations were initialized two days post-infection, which coincided with the time of viral burst and increment in bacterial densities relative to control cultures. To calculate the fraction of bacteria out of the total particulate organic matter we used the following equation:

$f_{\mathrm{phyto}} \cdot (\mathrm{C{:}\,N})_{\mathrm{phyto}} + f_{\mathrm{bacteria}} \cdot (\mathrm{C{:}\,N})_{\mathrm{bacteria}} = (\mathrm{C{:}\,N})_{\mathrm{POM}}$,

where $(\mathrm{C{:}\,N})_{\mathrm{phyto}}$, $(\mathrm{C{:}\,N})_{\mathrm{bacteria}}$, and $(\mathrm{C{:}\,N})_{\mathrm{POM}}$ are the C:N ratio in phytoplankton, bacteria, and POM, respectively. f_{phyto}, and f_{bacteria} are the fraction of phytoplankton and bacteria, respectively. Assuming that $f_{\mathrm{phyto}} + f_{\mathrm{bacteria}} = 1$, and rearranging, we get the following equation:

$$f_{\mathrm{bacteria}} = \frac{(\mathrm{C{:}\,N})_{\mathrm{POM}} - (\mathrm{C{:}\,N})_{\mathrm{phyto}}}{(\mathrm{C{:}\,N})_{\mathrm{bacteria}} - (\mathrm{C{:}\,N})_{\mathrm{phyto}}}$$

Here, $(\mathrm{C{:}\,N})_{\mathrm{phyto}}$= 8.32 is the ratio measured 48 hr post-infection (see Fig. 3 in the Results section). $(\mathrm{C{:}\,N})_{\mathrm{bacteria}}$= 4.94 is the average of elemental ratio of heterotrophic bacteria (Table S1; (43, 44) The $(\mathrm{C{:}\,N})_{\mathrm{POM}}$ is based on the results of our experimental findings (Fig. 5).

Acknowledgments

This study was supported by a scholarship from the Bester Award for Oceanography from the Hebrew University of Jerusalem attributed to TD, the Fulbright and Yad Hanadiv Fellowships attributed to SS, the Israel Science Foundation grant number 2921/20 attributed to MJF, the Israel Science Foundation grant number 2361/19 attributed to GA, and by the Natural Sciences and Engineering Research Council of Canada Discovery

grant (RGPIN-2022-04305) and Fonds de Recherche du Québec Relève Professorale grant (314248) attributed to AP. We thank Tania Rivlin for undertaking inorganic nutrient measurements and Gil Koplovitz for help during experiments. We finally thank Maoz Fine and Nir Keren for constructive feedback during the preparatory stages of the work.

Author Contributions: T.D., G.A. and M.J.F. conceptualized and designed the research; T.D., G.A., A.P., S.S. and M.J.F. performed research; G.A., A.P. and M.J.F. contributed analytic tools and funding; T.D., G.A., A.P., S.S. and M.J.F. analyzed data and revised paper drafts; T.D. and M.J.F. wrote the paper.

References

1. C. B. Field, M. J. Behrenfeld, J. T. Randerson, P. Falkowski, Primary Production of the Biosphere: Integrating Terrestrial and Oceanic Components. *Science (80).* **281**, 237–240 (1998).
2. J. L. Sarmiento, M. Bender, Carbon biogeochemistry and climate change. *Photosynth. Res.* **39**, 209–234 (1994).
3. D. A. Hutchins, M. R. Mulholland, F. Fu, Nutrient cycles and marine microbes in a CO2-enriched ocean. *Oceanography* **22**, 128–145 (2009).
4. P. G. Falkowski, T. Fenchel, E. F. Delong, The microbial engines that drive earth's biogeochemical cycles. *Science (80-.).* **320**, 1034–1039 (2008).
5. Z. V. Finkel, *et al.*, Phytoplankton in a changing world: Cell size and elemental stoichiometry. *J. Plankton Res.* **32**, 119–137 (2010).
6. C. Deutsch, T. Weber, Nutrient Ratios as a Tracer and Driver of Ocean Biogeochemistry. *Ann. Rev. Mar. Sci.* **4**, 113–141 (2012).
7. S. Sharoni, I. Halevy, Nutrient ratios in marine particulate organic matter are predicted by the population structure of well-adapted phytoplankton. *Sci. Adv.* **6**, 1–10 (2020).
8. E. D. Galbraith, A. C. Martiny, A simple nutrient-dependence mechanism for predicting the stoichiometry of marine ecosystems. *Proc. Natl. Acad. Sci. U. S. A.* **112**, 8199–8204 (2015).
9. J. A. Fuhrman, Marine viruses and their biogeochemical and ecological effects. *Nature* **399**, 541–548 (1999).

10. S. W. Wilhelm, C. A. Suttle, Viruses and Nutrient Cycles in the Sea. *Bioscience* **49**, 781–788 (1999).
11. K. D. A. Mojica, J. Huisman, S. W. Wilhelm, C. P. D. Brussaard, Latitudinal variation in virus-induced mortality of phytoplankton across the North Atlantic Ocean. *ISME J.* **10**, 500–513 (2016).
12. A. E. Zimmerman, *et al.*, Metabolic and biogeochemical consequences of viral infection in aquatic ecosystems. *Nat. Rev. Microbiol.* **18**, 21–34 (2020).
13. A. J. Poulton, T. R. Adey, W. M. Balch, P. M. Holligan, Relating coccolithophore calcification rates to phytoplankton community dynamics: Regional differences and implications for carbon export. *Deep. Res. Part II Top. Stud. Oceanogr.* **54**, 538–557 (2007).
14. A. J. Poulton, *et al.*, The 2008 *Emiliania huxleyi* bloom along the Patagonian Shelf: Ecology, biogeochemistry, and cellular calcification. *Global Biogeochem. Cycles* **27**, 1023–1033 (2013).
15. J. R. Young, S. A. Davis, P. R. Bown, S. Mann, Coccolith ultrastructure and biomineralisation. *J. Struct. Biol.* **126**, 195–215 (1999).
16. F. M. Monteiro, *et al.*, Why marine phytoplankton calcify. *Sci. Adv.* **2** (2016).
17. B. Rost, U. Riebesell, Coccolithophores and the biological pump: responses to environmental changes. *Coccolithophores*, 99–125 (2004).
18. C. Klaas, D. E. Archer, Association of sinking organic matter with various types of mineral ballast in the deep sea: Implications for the rain ratio. *Global Biogeochem. Cycles* **16**, 63-1-63–14 (2002).
19. J. L. Sarmiento, N. Gruber, Sinks for Anthropogenic Carbon. *Phys. Today* **55**, 30–36 (2002).
20. P. M. Holligan, *et al.*, A biogeochemical study of the coccolithophore, *Emiliania huxleyi*, in the North Atlantic. *Global Biogeochem. Cycles* **7**, 879–900 (1993).
21. T. Tyrrell, A. Merico, "*Emiliania huxleyi*: bloom observations and the conditions that induce them" in *Coccolithophores*, (Springer Berlin Heidelberg, 2004), pp. 75–97.

22. A. Winter, J. Henderiks, L. Beaufort, R. E. M. Rickaby, C. W. Brown, Poleward expansion of the coccolithophore *Emiliania huxleyi*. *J. Plankton Res.* **36**, 316–325 (2014).

23. E. J. Lessard, A. Merico, T. Tyrrell, Nitrate:phosphate ratios and *Emiliania huxleyi* blooms. *Limnol. Oceanogr.* **50**, 1020–1024 (2005).

24. G. Bratbak, J. K. Egge, M. Heldal, Viral mortality of the marine alga *Emiliania huxleyi* (Haptophyceae) and termination of algal blooms. *Mar. Ecol. Prog. Ser.* **93**, 39–48 (1993).

25. C. P. D. Brussaard, R. S. Kempers, A. J. Kop, R. Riegman, M. Heldal, Virus-like particles in a summer bloom of *Emiliania huxleyi* in the North Sea. *Aquat. Microb. Ecol.* **10**, 105–113 (1996).

26. W. H. Wilson, *et al.*, Isolation of viruses responsible for the demise of an Emiliania huxleyi bloom in the English Channel. *J. Mar. Biol. Assoc. United Kingdom* **82**, 369–377 (2002).

27. Y. Lehahn, *et al.*, Decoupling physical from biological processes to assess the impact of viruses on a mesoscale algal bloom. *Curr. Biol.* **24**, 2041–2046 (2014).

28. D. C. Schroeder, J. Oke, G. Malin, W. H. Wilson, Coccolithovirus (Phycodnaviridae): Characterisation of a new large dsDNA algal virus that infects *Emiliania huxleyi*. *Arch. Virol.* **147**, 1685–1698 (2002).

29. K. D. Bidle, L. Haramaty, J. Barcelos, P. Falkowski, Viral activation and recruitment of metacaspases in the unicellular coccolithophore, *Emiliania huxleyi*. **104** (2007).

30. A. Vardi, *et al.*, Viral Glycosphingolipids Induce Lytic Infection and Cell Death in Marine Phytoplankton. *Science (80-.).* **326**, 861–865 (2009).

31. U. Sheyn, S. Rosenwasser, S. Ben-Dor, Z. Porat, A. Vardi, Modulation of host ROS metabolism is essential for viral infection of a bloom-forming coccolithophore in the ocean. *ISME J.* **10**, 1742–1754 (2016).

32. D. Schatz, *et al.*, Hijacking of an autophagy-like process is critical for the life cycle of a DNA virus infecting oceanic algal blooms. *New Phytol.* **204**, 854–863 (2014).

33. S. Rosenwasser, *et al.*, Rewiring host lipid metabolism by large viruses determines the fate of Emiliania huxleyi, a bloom-forming alga in the ocean. *Plant Cell* **26**, 2689–2707 (2014).

34. S. Malitsky, *et al.*, Viral infection of the marine alga *Emiliania huxleyi* triggers lipidome remodeling and induces the production of highly saturated triacylglycerol. *New Phytol.* **210**, 88–96 (2016).

35. S. Jacquet, *et al.*, Flow cytometric analysis of an *Emiliana huxleyi* bloom terminated by viral infection. *Aquat. Microb. Ecol.* **27**, 111–124 (2002).

36. M. Trainic, *et al.*, Infection Dynamics of a Bloom-Forming Alga and Its Virus Determine Airborne Coccolith Emission from Seawater. *iScience* **6**, 327–335 (2018).

37. C. T. Johns, *et al.*, The mutual interplay between calcification and coccolithovirus infection. *Environ. Microbiol.* **21**, 1896–1915 (2019).

38. A. Vardi, *et al.*, Host-virus dynamics and subcellular controls of cell fate in a natural coccolithophore population. *Proc. Natl. Acad. Sci. U. S. A.* **109**, 19327–19332 (2012).

39. C. P. Laber, *et al.*, Coccolithovirus facilitation of carbon export in the North Atlantic. *Nat. Microbiol.* **3**, 537–547 (2018).

40. S. Rosenwasser, C. Ziv, S. G. van Creveld, A. Vardi, Virocell Metabolism: Metabolic Innovations During Host–Virus Interactions in the Ocean. *Trends Microbiol.* **24**, 821–832 (2016).

41. M. N. Müller, A. N. Antia, J. LaRoche, Influence of cell cycle phase on calcification in the coccolithophore *Emiliania huxleyi*. *Limnol. Oceanogr.* **53**, 506–512 (2008).

42. F. Vincent, *et al.*, Viral infection switches the balance between bacterial and eukaryotic recyclers of organic matter during algal blooms. *bioRxiv*, 2021.10.25.465659 (2021).

43. A. E. Zimmerman, S. D. Allison, A. C. Martiny, Phylogenetic constraints on elemental stoichiometry and resource allocation in heterotrophic marine bacteria. *Environ. Microbiol.* **16**, 1398–1410 (2014).

44. A. E. White, S. J. Giovannoni, Y. Zhao, K. Vergin, C. A. Carlson, Elemental content and stoichiometry of SAR11 chemoheterotrophic marine bacteria. *Limnol. Oceanogr. Lett.* **4**, 44–51 (2019).

45. M. Frada, I. Probert, M. J. Allen, W. H. Wilson, C. De Vargas, The “Cheshire Cat” escape strategy of the coccolithophore *Emiliania huxleyi* in response to viral infection. *Proc. Natl. Acad. Sci. U. S. A.* **105**, 15944–15949 (2008).

46. M. J. Frada, *et al.*, Morphological switch to a resistant subpopulation in response to viral infection in the bloom-forming coccolithophore *Emiliania huxleyi*. *PLOS Pathog.* **13**, e1006775 (2017).

47. C. Evans, G. Malin, G. P. Mills, W. H. Wilson, Viral infection of *Emiliania huxleyi* (Prymnesiophyceae) leads to elevated production of reactive oxygen species. *J. Phycol.* **42**, 1040–1047 (2006).

48. J. Kegel, *et al.*, Pilot study of an EST approach of the coccolithophorid *Emiliania huxleyi* during a virus infection. *Gene* **406**, 209–216 (2007).

49. S. A. Kimmance, M. J. Allen, A. Pagarete, J. M. Martínez, W. H. Wilson, Reduction in photosystem II efficiency during a virus-controlled *Emiliania huxleyi* bloom. **495**, 65–76 (2014).

50. C. A. Llewellyn, *et al.*, The response of carotenoids and chlorophylls during virus infection of *Emiliania huxleyi* (Prymnesiophyceae). *J. Exp. Mar. Bio. Ecol.* **344**, 101–112 (2007).

51. R. Riegman, W. Stolte, A. A. M. Noordeloos, D. Slezak, Nutrient uptake and alkaline phosphatase (ec 3:1:3:1) activity of emiliania huxleyi (Prymnesiophyceae)
during growth under n and p limitation in continuous cultures. *J. Phycol.* **36**, 87–96 (2000).

52. R. Geider, J. La Roche, Redfield revisited: variability of C:N:P in marine microalgae and its biochemical basis. *Eur. J. Phycol.* **37**, 1–17 (2002).

53. A. L. Pasulka, *et al.*, Interrogating marine virus-host interactions and elemental transfer with BONCAT and nanoSIMS-based methods. *Environ. Microbiol.* **20**, 671–692 (2018).

54. E. Yakubovskaya, T. Zaliznyak, J. M. Martínez, G. T. Taylor, Raman Microspectroscopy Goes Viral: Infection Dynamics in the Cosmopolitan Microalga, *Emiliania huxleyi*. *Front. Microbiol.* **12** (2021).

55. M. J. Allen, D. C. Schroeder, W. H. Wilson, Preliminary characterisation of repeat families in the genome of EhV-86, a giant algal virus that infects the marine microalga *Emiliania huxleyi. Arch. Virol.* **151**, 525–535 (2006).

56. W. H. Wilson, *et al.*, Complete genome sequence and lytic phase transcription profile of a Coccolithovirus. *Science (80-.).* **309**, 1090–1092 (2005).

57. M. J. Frada, *et al.*, Zooplankton may serve as transmission vectors for viruses infecting algal blooms in the ocean. *Curr. Biol.* **24**, 2592–2597 (2014).

58. A. Pagarete, *et al.*, Dip in the gene pool: Metagenomic survey of natural coccolithovirus communities. *Virology* **466**–**467**, 129–137 (2014).

59. C. J. Gobler, D. A. Hutchins, N. S. Fisher, E. M. Cosper, S. A. Sañudo-Wilhelmy, Release and bioavailability of C, N, P, Se, and Fe following viral lysis of a marine chrysophyte. *Limnol. Oceanogr.* **42**, 1492–1504 (1997).

60. F. Vincent, *et al.*, Viral infection switches the balance between bacterial and eukaryotic recyclers of organic matter during coccolithophore blooms. *Nat. Commun.* **14** (2023).

61. J. L. Clasen, J. J. Elser, The effect of host *Chlorella* NC64A carbon:phosphorus ratio on the production of *Paramecium bursaria Chlorella* Virus-1. *Freshw. Biol.* **52**, 112–122 (2007).

62. L. F. Jover, T. C. Effler, A. Buchan, S. W. Wilhelm, J. S. Weitz, The elemental composition of virus particles: Implications for marine biogeochemical cycles. *Nat. Rev. Microbiol.* **12**, 519–528 (2014).

63. M. G. Weinbauer, Ecology of prokaryotic viruses. *FEMS Microbiol. Rev.* **28**, 127–181 (2004).

64. M. B. Sullivan, J. S. Weitz, S. Wilhelm, Viral ecology comes of age. *Environ. Microbiol. Rep.* **9**, 33–35 (2017).

65. Z. V. Finkel, *et al.*, Phytoplankton in a changing world: cell size and elemental stoichiometry. *J. Plankton Res.* **32**, 119–137 (2010).

66. J. C. Nejstgaard, H. J. Witte, P. van der Wal, A. Jacobsen, Copepod grazing during a mesocosm study of an *Emiliania huxleyi* (Prymnesiophyceae) bloom. *Sarsia* **79**, 369–377 (1994).

67. M. B. Olson, S. L. Strom, Phytoplankton growth, microzooplankton herbivory and community structure in the southeast Bering Sea: insight into the formation and temporal persistence of an *Emiliania huxleyi* bloom. *Deep Sea Res. Part II Top. Stud. Oceanogr.* **49**, 5969–5990 (2002).

68. K. M. J. Mayers, *et al.*, Growth and mortality of coccolithophores during spring in a temperate Shelf Sea (Celtic Sea, April 2015). *Prog. Oceanogr.* **177**, 101928 (2019).

69. C. Evans, W. H. Wilson, Preferential grazing of *Oxyrrhis marina* on virus-infected *Emiliania huxleyi. Limnol. Oceanogr.* **53**, 2035–2040 (2008).

70. A. I. Vermont, *et al.*, Virus infection of *Emiliania huxleyi* deters grazing by the copepod *Acartia tonsa*. *J. Plankton Res.* **38**, 1194–1205 (2016).

71. A. G. Goode, D. M. Fields, S. D. Archer, J. M. Martínez, Physiological responses of oxyrrhis marina to a diet of virally infected *Emiliania huxleyi*. *PeerJ* **2019**, 1–25 (2019).

72. M. D. Keller, R. C. Selvin, W. Claus, R. R. L. Guillard, Media for the culture of oceanic ultraphytoplankton 1,2. *J. Phycol.* **23**, 633–638 (1987).

73. D. Marie, C. P. D. Brussaard, R. Thyrhaug, G. Bratbak, D. Vaulot, Enumeration of marine viruses in culture and natural samples by flow cytometry. *Appl. Environ. Microbiol.* **65**, 45–52 (1999).

74. M. Neder, R. Saar, A. Malik, G. Antler, T. Mass, New Insights on the Diurnal Mechanism of Calcification in the Stony Coral, Stylophora pistillata. *Front. Mar. Sci.* **8**, 1–15 (2022).

75. W. I. M. Holman, A new technique for the determination of phosphorus by the molybdenum blue method. *Biochem. J.* **37**, 256–259 (1943).

76. W. G. Crumpton, T. M. Isenhart, P. D. Mitchell, Nitrate and organic N analyses with second-derivative spectroscopy. *Limnol. Oceanogr.* **37**, 907–913 (1992).

77. D. M. Karl, B. D. Tilbrook, G. Tien, Seasonal coupling of organic matter production and particle flux in the western Bransfield Strait, Antartica. *Deep Sea Res. Part A. Oceanogr. Res. Pap.* **38**, 1097–1126 (1991).